



Suspension Plasma-Sprayed Thermal Barrier Coatings for Light-Duty Diesel Engines

Wellington Uczak de Goes¹ · Joop Somhorst² · Nicolai Markocsan¹ · Mohit Gupta¹ · Kseniya Illkova³

Submitted: 16 July 2019 / in revised form: 9 September 2019 / Published online: 2 October 2019
© The Author(s) 2019

Abstract Demands for improved fuel efficiency and reduced CO₂ emissions of diesel engines have been the driving force for car industry in the past decades. One way to achieve this would be by using thermal spraying to apply a thermal insulation layer on parts of the engine's combustion chamber. A candidate thermal spray process to give coatings with appropriate properties is suspension plasma spray (SPS). SPS, which uses a liquid feedstock for the deposition of finely structured columnar ceramic coatings, was investigated in this work for application in light-duty diesel engines. In this work, different spray processes and materials were explored to achieve coatings with optimized microstructure on the head of aluminum pistons used in diesel engine cars. The functional properties of the coatings were evaluated in single-cylinder engine experiments. The influence of thermo-physical properties of the coatings on their functional properties has been discussed. The influence of different spray processes on coating formation on the complex piston head profiles has been also discussed. The results show that SPS can be a promising technique for producing coatings on parts of the combustion chamber, which can possibly lead to higher engine efficiency in light-duty diesel engines.

Keywords diesel engines · fuel efficiency · microstructure · suspension plasma spraying · surface engineering · thermal barrier coatings

Introduction

The limited stores of fossil fuels are dwindling millions of times faster than they are formed, leading to availability problems soon. Moreover, when these fossil fuels are burned, greenhouse gases such as carbon dioxide (CO₂), methane (CH₄) and nitrous oxide (N₂O) are formed and emanated in the atmosphere, leading to greenhouse effect and climate changes with catastrophic consequences for life on Earth (Ref 1-3). The society nowadays is dependent on the internal combustion engines for the transport of goods and people. The global vehicle population was estimated to be 1.32 billion cars and trucks at the end of 2016, not counting the off-road vehicles or heavy machinery (Ref 4). According to the United States Environmental Protection Agency, combustion engines produce 27.7% of the greenhouse gas emissions in US (2017), while in Europe, they are responsible for 27% of the greenhouse gas emissions (2016) according to the European Environment Agency (Ref 5, 6). Therefore, methods to use fossil fuels in a sustainable and environmentally friendly way must be explored and implemented immediately.

One of the most straightforward ways is to increase the efficiency of the combustion engines. Ceramic thermal barrier coatings (TBCs) applied on combustion engine parts by thermal spraying have been receiving attention, especially in the case of diesel engines, for at least 30 years in order to improve engine efficiency. The advantages of using ceramic coatings are resistance to oxidation, stable microstructure, high resistance to thermal cycling and reduction of heat losses in the engine during operation, which could potentially lead to an increased engine efficiency and lower fuel consumption (Ref 7). However, the coatings produced and investigated as potential protective coatings for diesel engines have not shown promising

✉ Wellington Uczak de Goes
wellington.uczak-de-goes@hv.se

¹ University West, Trollhättan, Sweden

² Volvo Car Corporation, Göteborg, Sweden

³ Institute of Plasma Physics, Prague, Czech Republic

results (Ref 8–11). Combination of low-cycle fatigue (which relates to start and stop of the engine), penetration of combustion gases in the TBCs, and high-cycle fatigue (which is associated to the thermal loads inside the engine during combustion) induced severe coating surface cracking, microspallation and accelerated crack growth making the coating unsuitable for combustion engine applications (Ref 12).

The thermal spray method used in the past was atmospheric plasma spray (APS), which typically resulted in TBCs with high porosity and coating thickness. More recent studies revealed that rather thin coatings with a columnar microstructure, with coatings that follow the temperature of the transient chamber gases, could provide improved efficiency to diesel engines. Application of these coatings, developed by Toyota and termed as thermo-swing wall insulation technology, resulted in reduced heat loss through the combustion chamber wall without intake air heating, leading to a better efficiency of the engine (Ref 13). This was made possible by the quick adaptation of the coating surface temperature during every engine stroke (Ref 13). Andrie et al. (Ref 14) showed that a thin TBC with high porosity, low thermal diffusivity and low heat capacity is needed to achieve this improvement.

Suspension plasma spraying (SPS) has already showed excellent results as thermal barrier coatings (TBC) for gas turbine industry and its capacity to produce thin and porous coatings (Ref 15). Suspension plasma spray is a technique that uses a suspension of the powder as the feedstock, enabling thus usage of nano- and submicron-sized feedstock powder, and produces coatings with unique microstructures and improved thermal and mechanical properties as compared to standard thermal spray processes. The coatings produced by SPS can be thin with homogeneously distributed high porosity and provide a high strain tolerance under a thermal cyclic environment, which can contribute to an improved coating lifetime (Ref 16–18).

The typical material used as top coat in thermal barrier coatings is 8 wt.% yttria stabilized zirconia (YSZ) due to its exceptional thermo-mechanical properties at elevated temperatures. Apart from YSZ, another material that has an increasing interest for high-temperature coatings applications is gadolinium zirconate (GZO). GZO can produce coatings with lower thermal conductivity and higher phase stability as compared to YSZ. The disadvantage of GZO is that it has a lower fracture toughness than YSZ, thus being more prone to spallation when exposed to the thermal cyclic testing conditions in gas turbines (Ref 15). However, the application of GZO in a combustion engine environment has not been investigated.

The aim of this paper was to investigate YSZ and GZO TBCs produced by SPS and assess whether they bring benefits over the APS TBCs in light-duty diesel engines.

The TBCs were investigated in terms of thermo-physical properties, microstructure, porosity evaluation and functional properties assessment by single-cylinder engine testing. The influence of different spray processes on coating formation on the complex piston head profiles was also investigated.

Methods and Procedure

Sample Spraying

Four different set of samples were sprayed in this work as shown in Table 1. One set of samples was sprayed by APS using solid powder YSZ feedstock, and it was a standard TBC sprayed in the industry nowadays for gas turbine applications. This sample was considered as reference sample as it has similar microstructure and thermal properties with other samples used in the previous studies for diesel engine applications (Ref 13, 14). The second and the third TBCs were sprayed by SPS, both using YSZ suspension. The two SPS YSZ samples were sprayed with same spray parameters, only the thickness was varied. The fourth sample was sprayed by SPS using GZO suspension. More details about the samples are given in Table 1.

Round coupons of eutectic Al-12%Si alloy, 25.4 mm in diameter and 6 mm thick were used as substrate specimens. The substrates were grit-blasted using alumina grit to achieve a surface roughness of R_a around 3 μm . After the grit-blasting step, a bond coat layer was applied on the specimens. For spraying the bond coats, a M3 supersonic gun from Uniqucoat Technologies, USA equipped with a 4L4 ceramic nozzle and feedstock of NiCoCrAlY (AMDRY 386) powder (Oerlikon Metco), was used for the SPS samples. For the APS reference sample, the bond coat layer was applied by APS using a F4-MB gun from Oerlikon Metco, and NiCoCrAlY (AMPERIT 410) powder supplied by H.C. Starck.

The suspensions used for spraying the SPS top coats had a solid load of 25 wt.% in ethanol and a median particle size (D50) of around 500 nm, provided by Treibacher Industrie AG (Althofen, Austria) and available commercially with the name AuerCoat YSZ and AuerCoat Gd–Zr. For the APS top coat, the powder feedstock used was METCO 204 B-NS (Oerlikon Metco). The equipment used for the spraying of the APS top coat was F4-MB gun, and for the SPS top coat, an Axial III gun from Mettech Corp. equipped with a Nanofeed 350 suspension feed system was used.

Piston Spraying

For the single-cylinder engine test, three coatings were applied on the piston heads. The selected TBCs were as

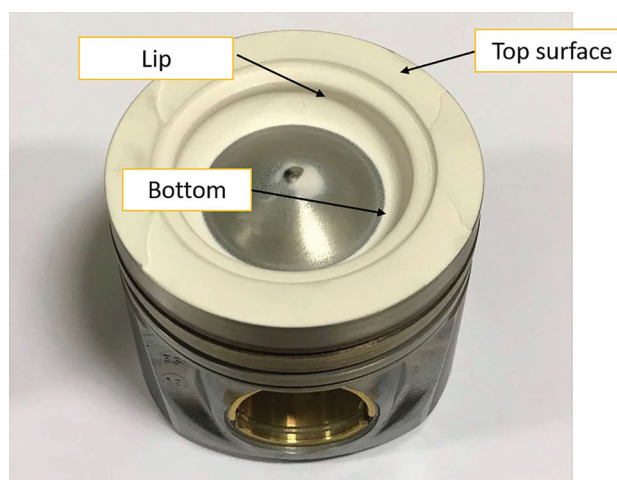
Table 1 Sprayed coatings

Abbreviation	Bond coat		Top coat		
	Process	Thickness, μm	Material	Process	Thickness, μm
APS YSZ	APS	109 ± 9	YSZ powder (METCO 204 B-NS)	APS	273 ± 10
SPS YSZ Thin	HVAF	132 ± 8	YSZ ethanol suspension 25 wt.%	SPS	243 ± 14
SPS YSZ Thick	HVAF	147 ± 11	YSZ ethanol suspension 25 wt.%	SPS	406 ± 10
SPS GZO	HVAF	149 ± 12	GZO ethanol suspension 25 wt.%	SPS	203 ± 7

follows: 1. YSZ sprayed by APS, 2. YSZ sprayed by SPS and 3. GZO sprayed by SPS, abbreviated as YSZ-APS, YSZ-SPS and GZO-SPS, respectively. Before spraying the coatings, the pistons were grit-blasted using alumina grit in order to achieve a proper roughness. Following the grit blasting, the bond coat layer was applied using the same materials and processes as for the coupons, with a target coating thickness of $120 \mu\text{m}$. After bond coat spraying, the ceramic coatings were sprayed using the same spray parameters, materials and processes as for the coupons with a target coating thickness of $250 \mu\text{m}$. As the spraying area on the piston was not plane, following the profile of the piston so that the spray angle is continuously kept perpendicular on the piston's surface was a challenge. To address this task, a spray routine was developed for all the spray processes and guns used to apply the TBCs on the pistons. The robot holding the spray gun was programmed to follow the piston's profile as much as possible while tilting the gun to keep the right angle as well as constant spray distance and traverse speed. The TBC coatings were not applied on the whole surface of the pistons but on a specific area that according to (Ref 19) is the hottest part on the piston during the combustion cycle. This area starts from the bottom of the piston head, going up over the lip (the most severe place), until the top surface of the piston. The faded white-colored coated area can be seen in Fig. 1.

Metallographic Preparation

After spraying, the samples underwent metallographic preparation in order to investigate the microstructure of the sprayed coatings. The procedure consists of first cold mounting in a low-viscosity epoxy resin under vacuum so that the resin can infiltrate the open porosity while avoiding damaging the coating. After first mounting, the samples were sectioned with the Struers Secotom 10 precision cutting machine equipped with an aluminum oxide cutoff wheel. The sample was then cold-mounted again with a high-viscosity resin, so it could fit in the Buehler Power Pro 5000 sample holder for further grinding and polishing making them ready for the microscopy analysis.

**Fig. 1** GZO SPS coating on light-duty diesel engine piston

To investigate the microstructure of the TBCs applied on pistons in both as-sprayed state and after the engine test, the pistons also underwent metallographic preparation. First, the bottom part of the piston was sectioned using a hacksaw. Then, the surface of the piston was covered with the low-viscosity epoxy resin under vacuum and then cured to preserve the coating's microstructure during subsequent sectioning. After this, the piston was sectioned with the Struers Secotom 10 precision cutting using the aluminum oxide cutoff wheel, as shown in Fig. 2, removing the selected region so the highlighted cross section could be investigated. The cutoff specimen was then cold-mounted with a high-viscosity resin, and then, same steps as for coupon were followed to prepare the coating surface for SEM analysis.

The polished samples were gold sputtered in order to make them suitable for SEM investigations. The SEM investigations were carried out with a SEM TM 3000 equipment from HITACHI.

Microstructure Analysis

The porosity measurements were carried out by image analysis employing ImageJ software. For the APS samples,



Fig. 2 Piston preparation, selected area

a single magnification image (500 ×) was used to measure the porosity content of the top coats. In the case of the SPS top coats, due to the very fine microstructural characteristics of the coatings (nano and micrometric pores), two different magnifications were used according to a procedure described in (Ref 13), i.e., a low magnification image (500 ×) capturing coarse porosity and a high magnification image (5000 ×) capturing fine porosity. To avoid the repetition of porosity in the images, a count mask of 2 μm² was used so that the low magnification images only considered pores bigger than 2 μm² and for the higher magnification images, only pores smaller than 2 μm² were considered. Ten images were taken per magnification along the surface of the sample to calculate the average porosity. The images were converted into black and white images (binary), and then, the porosity calculated. The total porosity for the APS samples was the average of the porosity results of all investigated microstructure images, whereas for the SPS samples, the total porosity was the sum of the average values of coarse and fine porosities.

The thickness of the samples was measured with a light optical microscope, BX60M from OLYMPUS. Ten thickness measurements were taken along each sample’s cross section, and the average of the measurements was taken as the final value.

Thermo-Physical Properties

The thermal diffusivity measurements were taken at the Institute of Plasma Physics, Czech Republic using an LFA

1000 Laser Flash Apparatus equipment from Linseis thermal analysis. In order to measure the thermal diffusivity, the sample needs to have the best absorption and emission properties. Therefore, the first step was to coat the sample with a thin layer of graphite. Then, the sample was positioned on a sample robot inside the equipment that is surrounded by a furnace. For the measurements, the furnace was held at a predetermined temperature (25, 100, 200, 300, 400 and 500 °C), and after achieving this desired sample temperature, a laser of known pulse irradiated the back side of the sample, resulting in a temperature rise at the sample surface. The resulting temperature rise of the surface of the sample was measured by a very sensitive high-speed IR detector, and the thermal diffusivity was calculated using Eq. (1)

$$\alpha = \frac{0.1388d^2}{t_{0.5}} \tag{Eq 1}$$

where α is the thermal diffusivity (mm²/s), d is the coating thickness (mm), and t_{0.5} is the half time taken for rise in temperature measured by the LFA equipment.

Linseis software model for the three different layers, the substrate, the bond coat and the ceramic top coat, with pulse correction was used for calculating thermal diffusivity. A zero-contact resistance between the different layers was considered for the purpose of simplification.

Thermal conductivity of the as-sprayed TBCs was calculated according to Eq. (2) at the temperature points previously established for the thermal diffusivity measurement (25, 100, 200, 300, 400 and 500 °C), using the corresponding thermal diffusivity and specific heat capacity values measured at those temperatures.

$$\lambda = \alpha \cdot C_p \cdot \rho \tag{Eq 2}$$

where λ is the thermal conductivity (W/(m.K)), α is the thermal diffusivity (mm²/s), C_p is the specific heat capacity (J/(gK)), and ρ is the coating density (g/cm³).

Density of the coatings (ρ) was calculated using the following equation:

$$\rho = (100 - \text{total porosity}(\%)) \cdot (\text{bulk density}). \tag{Eq 3}$$

The bulk density used in Eq. (3) was adopted as 6.1 g/cm³ for the YSZ and 6.32 g/cm³ for the GZO (Ref 15), and the values for specific heat capacity were adopted from the previous measurements done by differential scanning calorimetry.

The effusivity of the coating was calculated as shown in Eq. (4).

$$e = \sqrt{\lambda \cdot \rho \cdot C_p}. \tag{Eq 4}$$

Engine Testing

The engine test experiments of the pistons were performed in a single-cylinder light-duty diesel engine at Volvo Cars, Gothenburg. The engine was operated in four regimes, e.g., low, medium and high load point at 1500 rpm and one high load point at 3000 rpm. Each load point was run for about 35 min while taking measurements. The cylinder pressure and fuel consumption were measured to evaluate the engine efficiency and the heat losses from the combustion chamber.

The engine efficiency was calculated from the work on the piston, according to Eq. 5 and 6, where p (bar) is the cylinder pressure and V (cm³) is the cylinder volume.

$$\text{Work} = \int_{-180}^{180} p dV \quad (\text{Eq 5})$$

$$\text{efficiency} = \frac{\text{Work}}{\text{Fuel Energy}}. \quad (\text{Eq 6})$$

The heat losses were derived from the difference between the heat input from the combusted fuel and the apparent heat released. The apparent heat released was calculated according to Eq. 7, where the value for the specific heat ratio κ is a function of temperature and gas composition. Further information about this method can be found in the work done by Heywood (Ref 20).

$$\text{apparent heat released} = \int \left(\frac{\kappa}{\kappa - 1} p dV + \frac{1}{\kappa - 1} V dp \right);$$

$$\kappa = \frac{c_p}{c_v}. \quad (\text{Eq 7})$$

Results and Discussion

As-Sprayed Microstructure

Figure 3 presents cross-sectional SEM micrographs of the as-sprayed YSZ APS, SPS YSZ thin, YSZ SPS thick and SPS GZO samples. A few general characteristics can be observed such as a good interface between the substrate and the bond coat as well as between the bond coat and the top coat in all the coatings. A continuous contact at the different interfaces is a good premise for coatings with good adhesion and thus increased functional performances. Another general characteristic is the roughness of the different TBCs. While the roughness of the SPS TBCs is mainly given by the columnar structure of the coatings, the roughness of the APS TBC is given by the splats formed by the molten particles under impact. High roughness of the

top coats is typically not desired for TBCs used for automotive applications as it may negatively affect the combustion process (Ref 13).

It can be clearly seen in Fig. 3 that the microstructures of the APS and SPS TBC are significantly different. The APS coatings reveal a lamellar structure showing that the coating was built-up by splats that impacted over each other. This feature affects the thermal properties of the coating as in a lamellar structure the delamination type of pores (horizontally elongated voids) is typically formed as can be also seen in Fig. 4. The heat flux through such types of pores is significantly reduced, and thus, the thermal conductivity of the whole coating is lowered. The negative side of the delamination-type pores is that horizontal cracks can easily propagate through them, which can lead to premature failure of the coating.

The microstructure of the SPS coating, Fig. 5 and 6, exhibits a variety of features as also described in (Ref 21). The SPS TBCs reveal typical microstructural features such as columns, column gaps and a large variety of pores in terms of size, from very fine (nanometric pores) to larger ones (micrometric size) as indicated in Fig. 5. The YSZ SPS coatings in this study revealed all these features, and based on the region within the column as well as the area of the inter columnar spacing, these coatings can be categorized as having a columnar feathery microstructure. The GZO TBC reveals a more porous microstructure with columns that tend to widen toward the top of the coating. These features can be correlated with the different feedstock and deposition conditions as compared to those employed for producing the YSZ TBCs.

Figure 6 shows the cross section of the YSZ SPS thick at a higher magnification. Since the same parameters were used to spray this coating as the YSZ SPS thin, there are no apparent differences between the microstructure of the coatings. The only difference is that the YSZ SPS thick sample has almost double thickness as compared to YSZ SPS thin.

Figure 7 shows the cross section of the GZO SPS at higher magnification. The images show, even for a different type of feedstock, the typical microstructural features of SPS coatings. The differences that can be observed as compared to the YSZ-SPS sample are slightly wider columns and more feathery than YSZ SPS, the column gaps that are also wider and the pores that are larger, indicating a higher total porosity. As also pointed out above, these changes can be attributed to the different spray settings (adapted to GZO material) for the GZO samples as compared to YSZ samples and different melting points of GZO and YSZ.

The microstructure of the TBC coatings applied on pistons was also evaluated. This investigation was carried

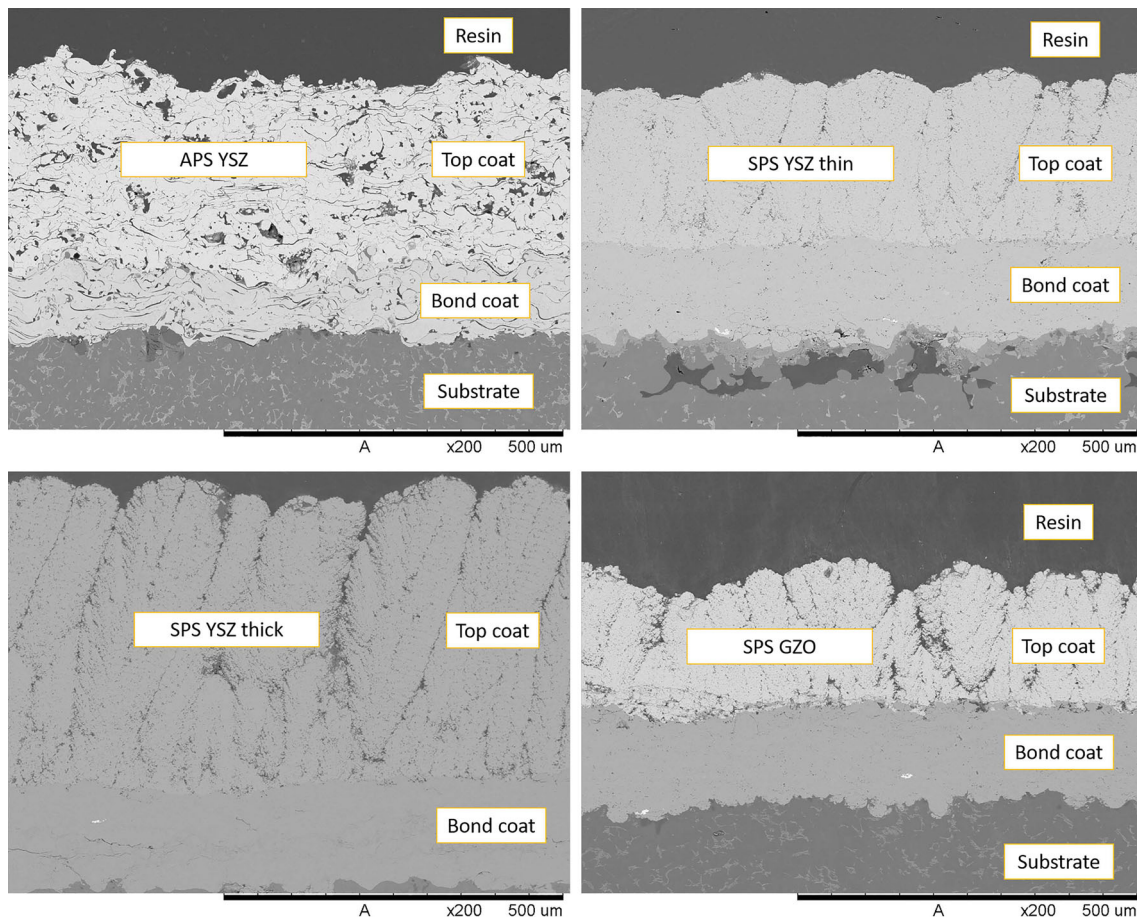


Fig. 3 YSZ APS, SPS YSZ thin, SPS YSZ thick and SPS GZO with $\times 200$ magnification, respectively

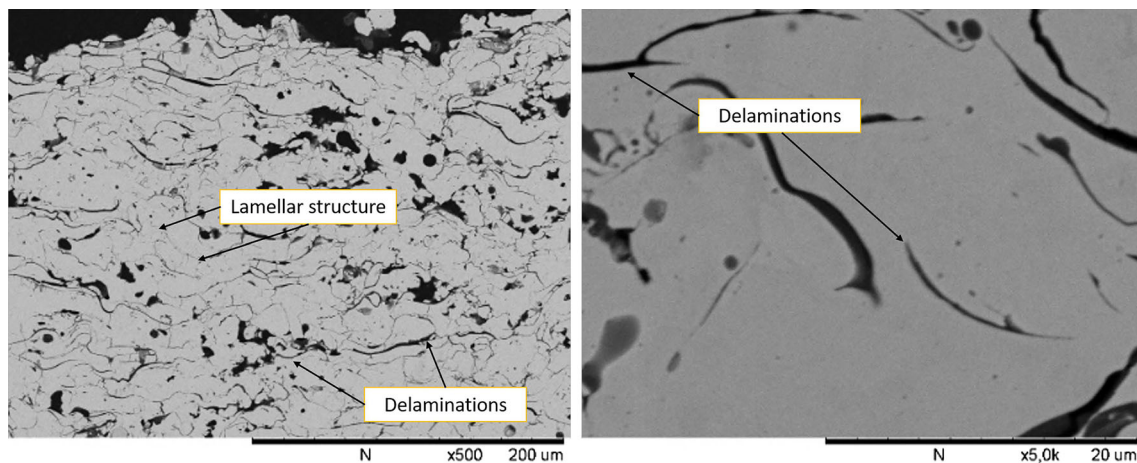


Fig. 4 APS YSZ with $\times 500$ and $\times 5000$ magnification

out in relation to the typical profile of the piston, and hence, the coatings sprayed on different type of surfaces (plane, concave, convex) and under different spray directions. In Fig. 8, the schematic profile of the investigated piston is presented along with microstructure images of the sprayed coatings on the corresponding areas. The typical

columnar microstructure of the SPS TBC and the dense microstructure of the HVAF bond coat can be seen along the whole profile of piston. The microstructures images in Fig. 8 also reveal the challenges and difficulties posed when the surface to be sprayed is not plane and/or spraying cannot be done on a normal direction to the surface to be

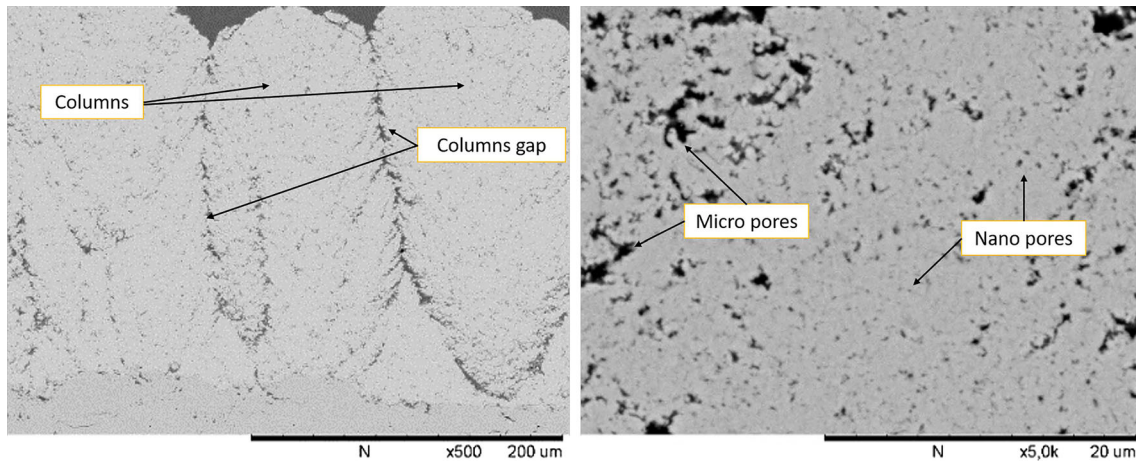


Fig. 5 YSZ SPS thin with $\times 500$ and $\times 5000$ magnification

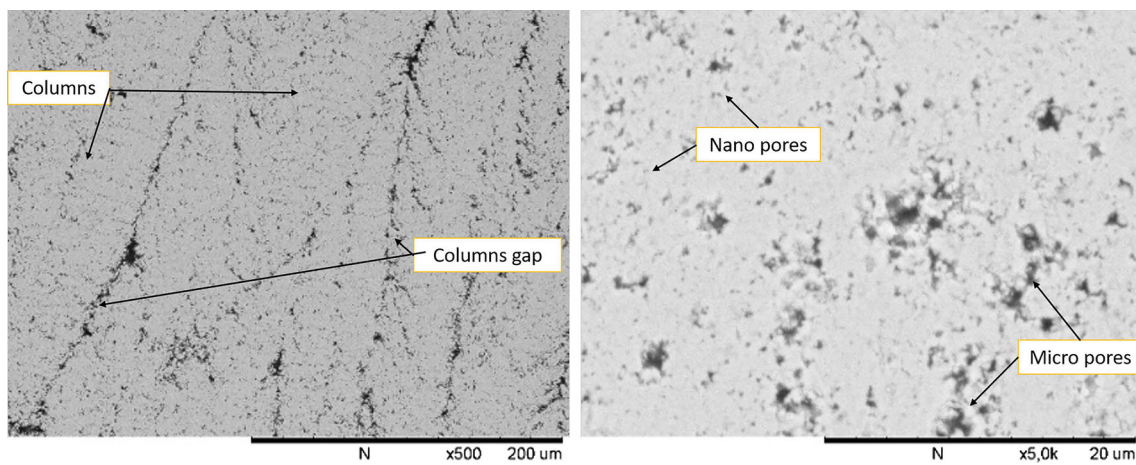


Fig. 6 YSZ SPS thick with $\times 500$ and $\times 5000$ magnification

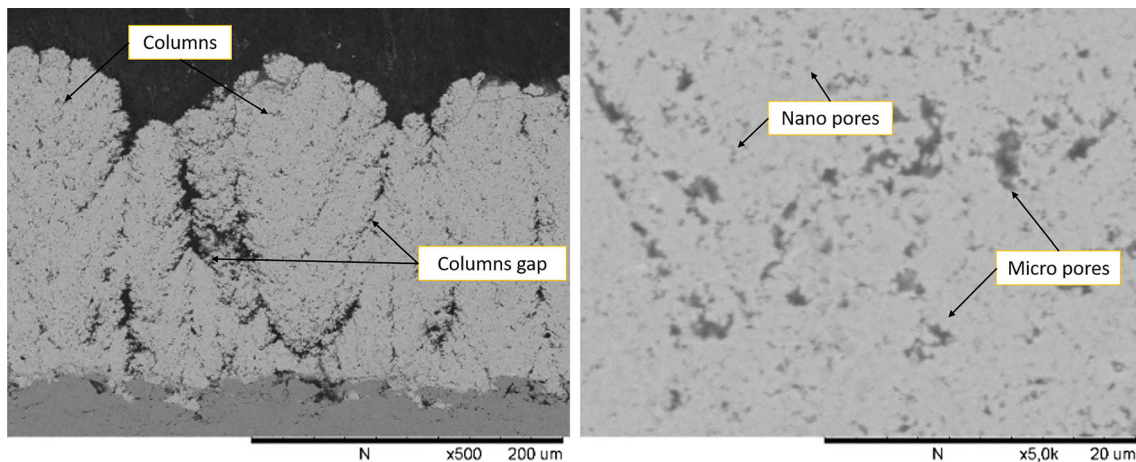


Fig. 7 GZO SPS with $\times 500$ and $\times 5000$ magnification

sprayed. Variable spray angles and spray distances as well as abrupt changes of the surface planarity, i.e., plane–concave–convex, horizontal–vertical had significant

influence on the applied coating's microstructure but more than that on the resulting thickness of the coatings, as shown in Table 2.

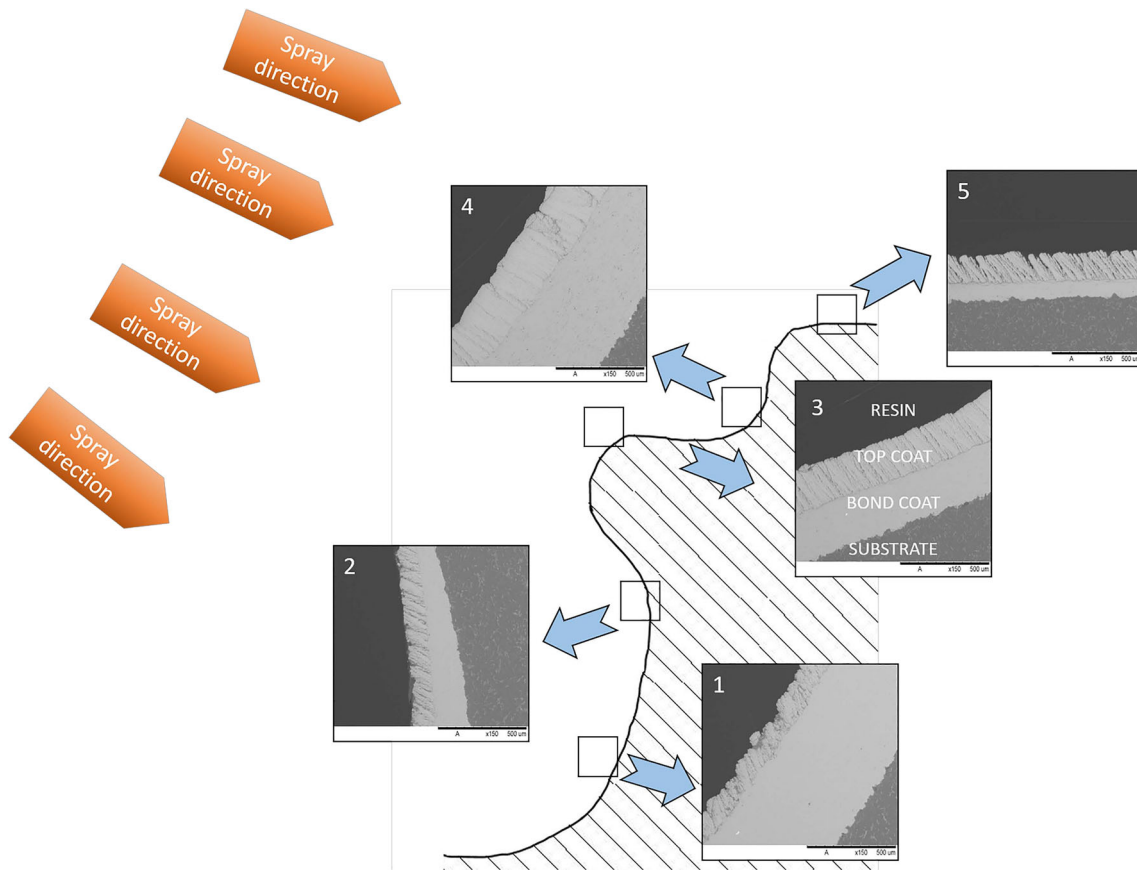


Fig. 8 YSZ SPS with $\times 150$ magnification along the different surfaces of the piston

As presented in Fig. 8 and in the Table 2, in region 1, the HVOF bond coat revealed a high thickness since the tilting of the gun in this region had an approximate 90° angle to the surface to be sprayed, leading to a higher deposition rate. Moreover, the concave substrate has probably helped in re-spraying the typically bounced-off particle so that the process efficiency was even higher. The

SPS TBC has preserved its columnar feathery microstructure but also showed a small inclination of the columns, due to the shape of the piston that influenced the column and consequently the coating formation. Formation of tilted columns when the spray direction is not perpendicular to the substrate’s surface has been demonstrated in the previous study done by Ganvir et al. (Ref 18). In region 2, since the spraying angle was much lower as compared to region 1, the deposition efficiency of the HVOF process became lower and the thickness as well. In the case of the SPS coatings due to the fact that the formation of the columns is based on the particles that are dragged by the plasma and column form along the plasma flow over the surface (not in the axis of the plasma stream), the steep spraying angle was not that problematic as for HVOF. Columns could still form and build up the coating, but to a relatively lower thickness with inclination. In region 3, the spray angle was relatively normal to the surface, but the shape of the spray area is concave. Thus, the HVOF process had a medium deposition rate, and relatively same spray conditions and deposition rate for the SPS process as well, with a small inclination of the columns of the TBCs. In region 4, again the angle of the spray direction and the surface of the piston was close to 90° and the surface shape

Table 2 Thickness of the different regions on the piston coating before testing

Region	Layer	Thickness, μm
1	Bond coat	407 ± 23
	Top coat	137 ± 9
2	Bond coat	154 ± 21
	Top coat	114 ± 12
3	Bond coat	225 ± 12
	Top coat	191 ± 5
4	Bond coat	487 ± 14
	Top coat	249 ± 14
5	Bond coat	78 ± 8
	Top coat	128 ± 11

was concave, which resulted in higher deposition rate for the HVAF process and a higher-thickness bond coat. Similarly, the SPS coating thickness was highest as compared to the other regions and the columnar microstructure with closely packed columns tending to dense vertical cracks TBCs (Ref 18). This kind of microstructure is believed to form due to the almost normal spray direction and the concave surface of the piston. In region 5, the spray direction was not a 90° angle and thus the deposition rate decreased again in the case of HVAF, leading to a lower thickness of the bond coat. The SPS TBC in this region had been formed in quite similar condition as it was discussed in region 2, i.e., a porous columnar coating with the columns tilted in direction of the spray stream.

As can be seen in the microstructure picture presented in Fig. 8 and the data from Table 2, the SPS process is not as sensitive as the HVAF process in terms of coating build-up and deposition efficiency when spraying surfaces of different shapes and/or the spraying is not done perpendicular on the area to be sprayed. The coating thickness variations of SPS TBC were not as dramatic as for HVAF bond coats. On the other hand, the variation in microstructural features formed due to different spray angles was much higher in the case of SPS coatings as compared to HVAF coatings. This difference is believed to come from the mechanisms the two processes build up the coating. The HVAF is a line-of-sight process that uses semi-molten particles and high-velocity spraying. In these conditions, if the surface is not normal to the spray direction, the particles can easily rebound or bounce-off when they impact the substrate. In SPS process, as also described above and studied elsewhere (Ref 18), the coating forms by particles which follow the plasma stream and hit the substrate away from the axis of the plasma stream. This mechanism seems to be effective when spraying needs to be done under conditions those described above.

Porosity

Figure 9 shows the porosity of the investigated samples. The porosity values of the SPS TBCs are divided into two categories for each sample, i.e., coarse porosity that is pores with area larger than $2 \mu\text{m}^2$ measured with images taken at $500 \times$ and fine porosity that is the pores with area smaller than $2 \mu\text{m}^2$ measured with images taken at $5000 \times$.

Due to the absence of the fine porosity in standard YSZ APS, only the coarse porosity was measured and shown. Analyzing the porosity results, it can be seen that the fine pores in the SPS coatings represent almost half of the total porosities. The lowest porosity was in the YSZ APS. The next lowest value of porosity was showed by the two YSZ SPS samples which showed similar porosity, as they were sprayed with the same spray parameters. The highest

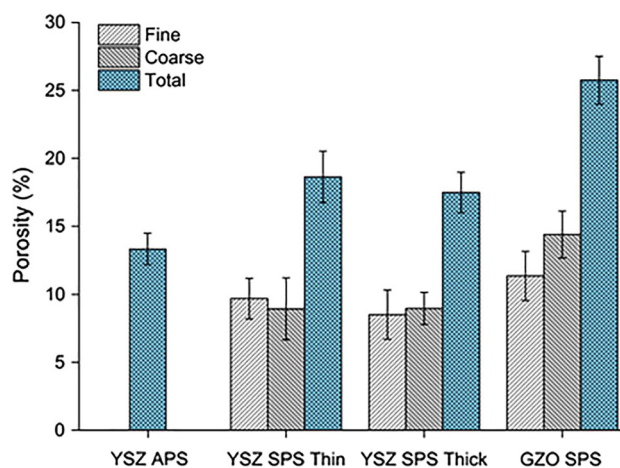


Fig. 9 Porosity of the coatings

porosity was shown by the GZO SPS coating, with more than half of the total porosity consisting of pores smaller than $2 \mu\text{m}^2$. These observations correlate well with the discussions in Sect. 3.1.

Thermal Properties

Thermal conductivity is an important material property for coatings used for high-temperature applications and is the first investigated property when the thermal insulation aptitude of a coating is investigated. The thermal conductivity in this study was calculated using Eq. (2) in the temperature range of 25 to 500 °C and is depicted in Fig. 10.

The thermal conductivity of the APS-sprayed coating revealed the lowest values probably because of its lamellar microstructure with delamination acting as barrier to the heat flow. Among the SPS coatings, the lowest thermal conductivity was shown by the SPS GZO coating. This result can have several reasons, as mentioned above the GZO coatings had a higher porosity but also the material itself has a lower thermal conductivity as compared to YSZ material. The previous studies (Ref 15) showed that the lower thermal conductivity of GZO can be related to the differences in crystallographic structures of the two materials. The different crystallographic structures of the GZO, as compared to YSZ, lead to different phonon scattering phenomena. More exactly, the two materials have distinct arrangement of the cations and oxygen vacancies, and thus if there is a larger number of oxygen ion vacancies in the crystallographic structure (GZO contains 33 mol.% of Gd_2O_3 whereas YSZ has 5 mol.% of Y_2O_3) a higher phonon scattering will occur, which will lead to a lower thermal conductivity. Another observation from Fig. 10 is that the thermal conductivity decreased as the temperature increased for all samples. The same behavior was reported

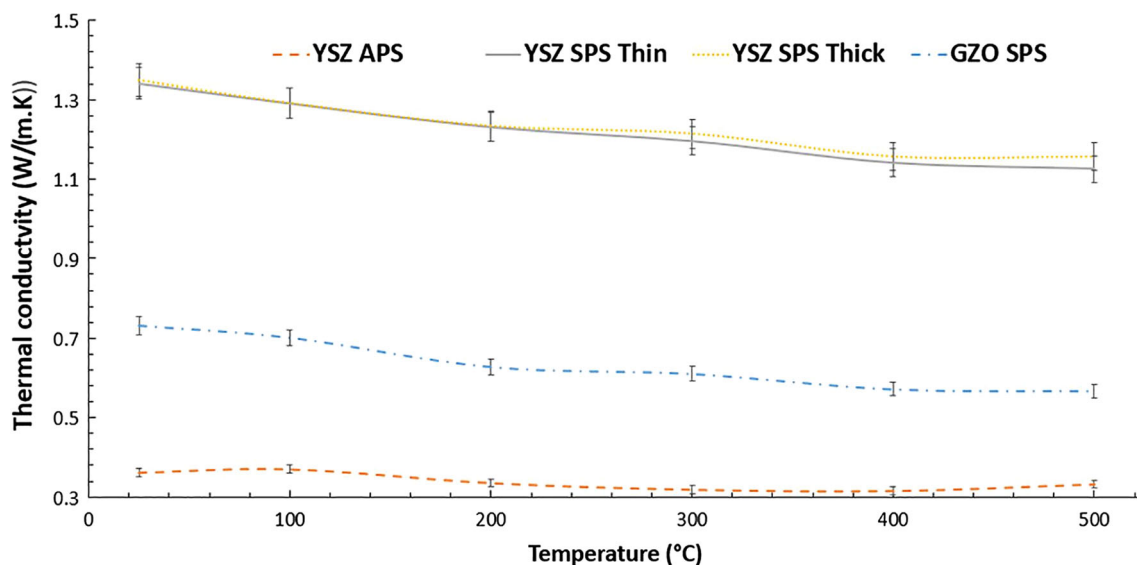


Fig. 10 Thermal conductivity of the as-sprayed coatings

previously (Ref 15, 22, 23), and related to phonon scattering in the ceramic layers that increases with the temperature and thus leading to a lower thermal conductivity. As both YSZ SPS samples, i.e., thick and thin, had the same microstructure, the measured thermal conductivity values were also almost identical as expected.

In real working conditions, the temperature to which the coatings are exposed may not be reaching a steady state, and thus only thermal conductivity properties of a coating might not be descriptive enough to understand the coating's behavior in such working environments. In this case, effusivity could be used. Effusivity of a coating is a measure of its ability to exchange thermal energy with the working environment. In other words, effusivity governs how fast the material absorbs and let the heat go, whereas the thermal conductivity is the property of a material to conduct heat (Ref 24).

The thermal effusivity of the four TBCs was calculated for the same range of temperature as for thermal conductivity, and the results are shown in Fig. 11. Due to the characteristic of the APS-sprayed samples, i.e., a lamellar structure, the low effusivity was expected. The APS values were followed closely by the GZO SPS coating and after that the highest effusivity was shown to be from the YSZ SPS thick and thin coatings. As both YSZ SPS samples showed similar microstructural features, the effusivity was expected to be not far from each other through the whole range of temperature. The lower effusivity value of the SPS GZO sample could be attributed to the higher porosity of the GZO SPS coatings but this behavior might be also associated with the characteristics of GZO, which has a lower thermal conductivity in bulk when compared to YSZ

(Ref 4). However, the difference between the effusivity of the SPS GZO and the APS YSZ is not yet so high than in the case of thermal conductivity values. The thermal conductivity of the APS TBC was almost half of that of SPS GZO whereas the effusivity values of the two coatings were much closer.

Engine Testing

The engine testing results are shown in Fig. 12 and 13. In Fig. 12, the heat loss of the engine in a single-cylinder test at the medium load point engine (load 50%) and engine speed of 1500 rpm is presented. The coated pistons are compared to a reference, which in this case was an uncoated piston. All TBCs revealed lower heat losses than the reference piston. The best performer in this test was the SPS GZO that had around 0.7% lower heat losses to the combustion chamber walls as compared to the reference piston. The SPS GZO was followed by the YSZ APS coating, and then, the lowest reduction was showed by the YSZ SPS. This test has a major significance as the additional heat energy can be converted into useful work that can lead to an increase in the engine's power and the efficiency. With the reduction of the heat transfer, the exhaust gas temperatures are prone to be higher, which gives the possibility of recovering the energy with the use of a turbocharger.

Following the same tendency as presented in Fig. 12, the indicated efficiency (power produced by the engine without frictional losses) is shown in Fig. 13. The results presented in Fig. 12 show an increased efficiency of the SPS GZO coating with 0.5% as compared to the reference

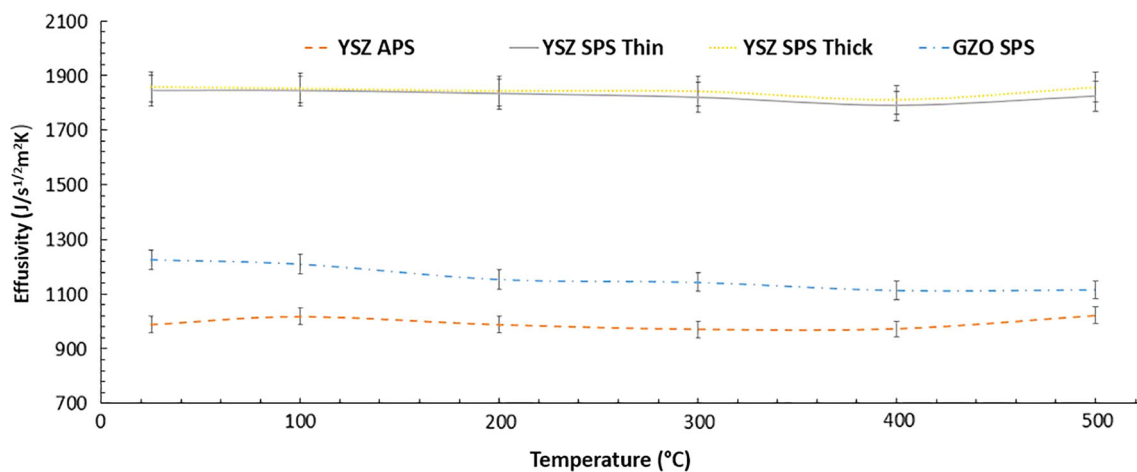


Fig. 11 Thermal effusivity of the as-sprayed coatings

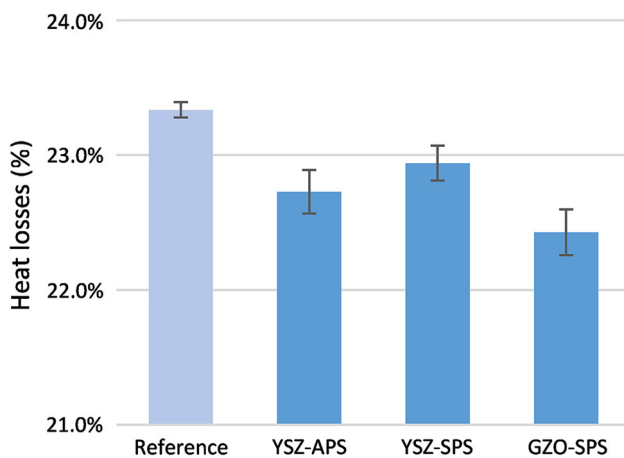


Fig. 12 Engine heat losses compared to an uncoated piston

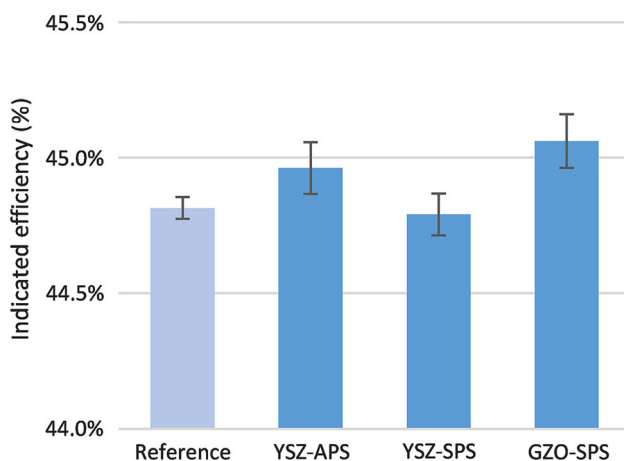


Fig. 13 Engine efficiency, compared to an uncoated piston

piston. SPS GZO coating was followed by the APS YSZ and the SPS YSZ coating.

The SPS GZO coating showed the best insulating performance not only in the test depicted in Fig. 13 but also for all engine operating points. The coatings performances in the engine could be partially aligned with the measured thermal conductivity and effusivity. If comparing only the SPS TBC coatings, it is quite clear that the SPS GZO showed the best thermal properties (conductivity and effusivity) and also best engine test results (heat losses and efficiency). However, when the SPS TBC is compared to the APS TBC, the thermal property results are not in concordance with the engine test results, i.e., the APS YSZ had lowest thermal conductivity and effusivity but not the best engine test performance. Although the reason of these results is not yet clear and needs further investigations, there might be some explanations.

The differences between the effusivity of the APS YSZ and the SPS TBCs are not as large as the difference between the thermal conductivity of the same coatings. This improvement in effusivity of the SPS TBCs can be related to the characteristic feature of the SPS coatings, i.e., a columnar microstructure, that exhibits a larger surface area as compared to APS coating, which has high porosity but a flatter surface. The larger surface area of the SPS coatings can quicker absorb and dissipate the heat (showed also by the effusivity results), whereas in APS TBC, this absorption and release of heat are delayed as the gases enter and exit the coating through the open pores and in time may heat up more the coating, as compared to the SPS TBC. Another reason for better engine test performance of the SPS TBC as compared to APS TBC might the higher amount of closed and very fine pores in SPS TBC. As also observed in the previous studies (Ref 25), the nanoporosities, present in a much higher amount in SPS TBC than in APS TBCs, could have contributed to an increased resistance of the SPS TBC to be heated up by combustion gases.

Coatings Microstructure After the Engine Test

The microstructure of the three TBCs along with the microstructure of a SPS YSZ piston that was not tested is

shown in detail in Table 3, and the thickness variation along the different regions is shown in Table 4. The microstructure images are tilted following the piston profile as shown in the schematic presented in Fig. 8.

Table 3 Microstructure of the different regions on the piston coating before and after testing

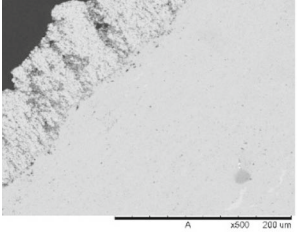
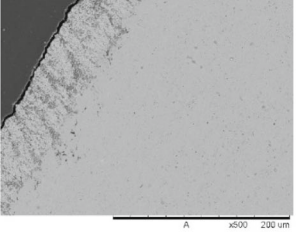
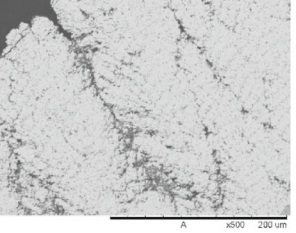
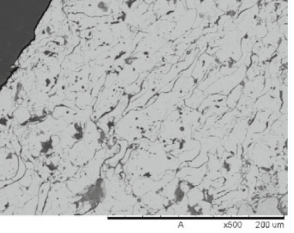
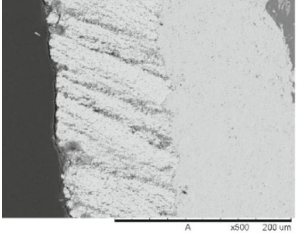
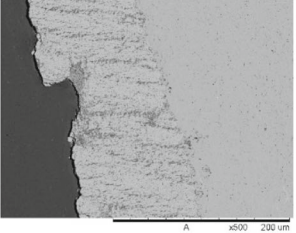
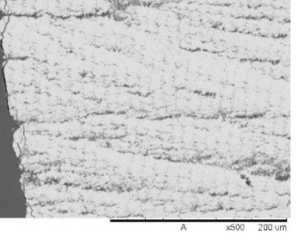
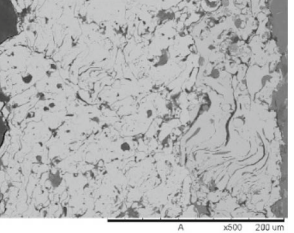
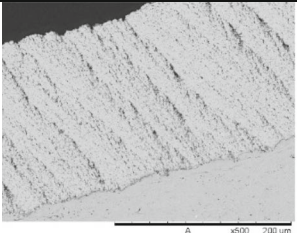
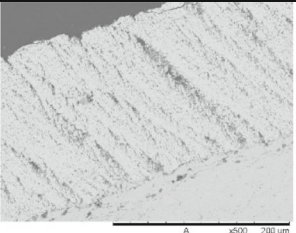
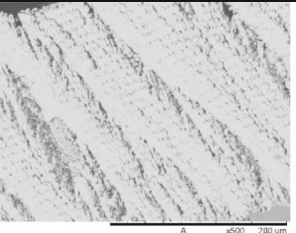
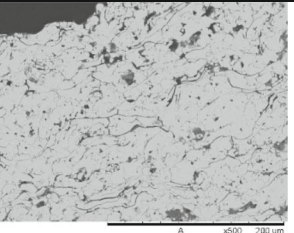
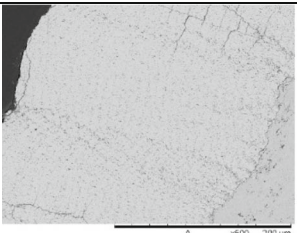
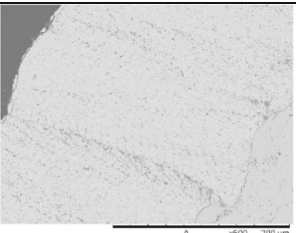
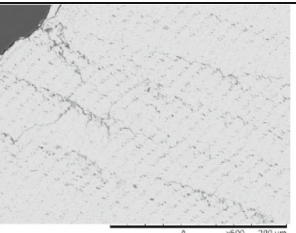
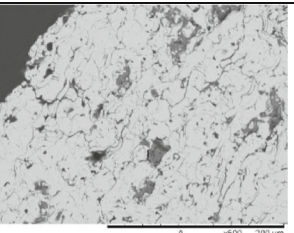
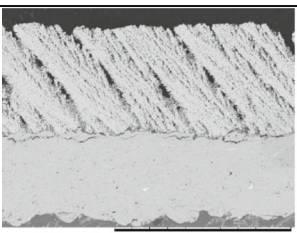
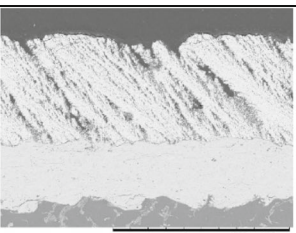
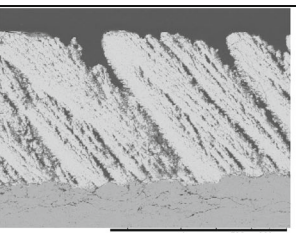
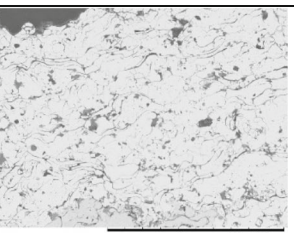
	Before testing	After testing		
Rg	YSZ SPS	YSZ SPS	GZO SPS	YSZ APS
1				
2				
3				
4				
5				

Table 4 Thickness of the different regions on the piston coating after testing

APS YSZ			SPS YSZ			SPS GZO		
Region	Layer	Thickness, μm	Region	Layer	Thickness, μm	Region	Layer	Thickness, μm
1	Bond coat	189 ± 18	1	Bond coat	518 ± 15	1	Bond coat	513 ± 11
	Top coat	266 ± 16		Top coat	117 ± 10		Top coat	366 ± 10
2	Bond coat	79 ± 23	2	Bond coat	148 ± 21	2	Bond coat	146 ± 13
	Top coat	215 ± 30		Top coat	109 ± 11		Top coat	360 ± 22
3	Bond coat	150 ± 18	3	Bond coat	216 ± 7	3	Bond coat	216 ± 7
	Top coat	352 ± 18		Top coat	187 ± 7		Top coat	288 ± 3
4	Bond coat	110 ± 9	4	Bond coat	457 ± 21	4	Bond coat	455 ± 13
	Top coat	320 ± 30		Top coat	245 ± 13		Top coat	378 ± 18
5	Bond coat	105 ± 10	5	Bond coat	79 ± 3	5	Bond coat	89 ± 4
	Top coat	271 ± 13		Top coat	127 ± 11		Top coat	161 ± 8

It can be seen in the pictures presented in Table 3 and the measurements in Table 4 that the features related to the spray direction and the shape of the piston remain similar with those presented in Fig. 8 and Table 2 as discussed in Sect. 3.1. When it comes to angles between the spray direction and the surface close to 90° , the HVOF process achieved a higher deposition efficiency while it decreased when spraying was done at lower spray angles. In the case of SPS coatings, as discussed earlier, the inclination of the columns was strongly dependent on the spray direction. Same microstructures as observed in Fig. 8, were observed on tested coatings (presented Table 3), i.e., the feathery columnar microstructure in region 1, columnar microstructure in regions 2, 3 and 5 and the columnar microstructure close to a dense vertically cracked in region 5. The APS coatings showed higher deposition efficiency in the regions 1, 3 and 4, with lesser variations in thickness in other regions unlike HVOF coatings. The better deposition efficiency of APS coatings could have been due to better melting of the particles in APS as compared to HVOF, resulting in lesser particles being bounced-off the substrate. For the HVOF process, higher deposition efficiency on the regions 1 and 4, which were normal to the spraying direction, was found. The SPS GZO process had a better deposition rate than SPS YSZ. This can be due to the fact that GZO usually has a higher deposition rate of $1 \mu\text{m}$ per pass as compared to YSZ, due to the lower melting temperature of GZO as compared to YSZ. This characteristic will make the GZO splats adhere in a higher number than the YSZ resulting in a higher thickness/pass. The higher thickness of the GZO coating could have also contributed to the better engine performance of this piston as a thicker layer would provide better insulation properties.

The images presented in columns 2 and 3 in Table 3 and the measurements in Table 4 illustrate the microstructure

of the TBCs before and after the engine test. No obvious differences could be seen comparing the two sets of microstructures.

Although the experiments were short in time (2 h and 10 min fired operation), the number of combustion cycles was just over 130,000, with 35 min and 52,250 cycles at near maximum power conditions, no visible damage was found in the coatings. Further durability testing is still required, but these initial tests are encouraging.

Conclusions

In this work, an experimental study was carried out on three types of TBC coatings to assess their properties (porosity, thermal conductivity and effusivity) and functional performances as protective layers in diesel engines. The results showed that:

- SPS GZO showed lower thermal conductivity than SPS YSZ, but higher than the APS YSZ.
- The effusivity calculations showed much closer values between the APS TBC and SPS TBCs than between the thermal conductivity values of the same samples.
- The best engine test result was revealed by the SPS GZO indicating it as promising coating material for diesel combustion engines. These results could be due to the columnar microstructure and the closed porosity that are characteristics of the SPS-sprayed coatings.
- No damage was observed on any of the tested TBC after running a full load engine test.
- There are microstructural differences between the coatings applied on the coupons specimen and those applied on pistons. These differences are due to the different spray directions and the curved shape of the piston.

The sample properties combined with the engine test results indicate that it is possible to have a better fuel efficiency with the use of ceramic coatings applied on the piston crown. The concept of using SPS coatings inside combustion engines demonstrated that a columnar microstructure with a higher porosity and lower thermal conductivity produced a lower heat loss and higher efficiency engine. This idea will be expanded and deepened in further studies.

Acknowledgments Open access funding provided by University West. The authors would like to thank Stefan Björklund from University West, Trollhättan to help in planning the spray trials for all the samples. Authors also gratefully acknowledge the Swedish Energy Agency for their support for this work, part of the FFI Energy & Environment Program.

Open Access This article is distributed under the terms of the Creative Commons Attribution 4.0 International License (<http://creativecommons.org/licenses/by/4.0/>), which permits unrestricted use, distribution, and reproduction in any medium, provided you give appropriate credit to the original author(s) and the source, provide a link to the Creative Commons license, and indicate if changes were made.

References

1. J.B. Goodenough, Energy Storage Materials: A Perspective, *Energy Storage Mater.*, 2015, **1**, p 158-161
2. R. Sathre, Comparing the Heat of Combustion of Fossil Fuels to the Heat Accumulated by their Lifecycle Greenhouse Gases, *Fuel*, 2014, **115**, p 674-677
3. W.K. Darkwah, B. Odum, M. Addae, D. Koomson, B. Kwakye Danso, E. Oti-Mensah, T. Asenso, and B. Adormaa, Greenhouse Effect: Greenhouse Gases and Their Impact on Global Warming, 2018.
4. S. Petit, World Vehicle Population Rose 4.6% in 2016, 2017, <https://subscribers.wardsintelligence.com/analysis/world-vehicle-population-rose-46-2016>. Accessed 10 July 2019.
5. United States Environmental Protection Agency, Overview of Greenhouse Gases, 2017, <https://www.epa.gov/ghgemissions/overview-greenhouse-gases>. Accessed 10 July 2019.
6. European Environment Agency, Greenhouse Gas Emissions from Transport, 2018.
7. M. Vittal, J.A. Borek, D.A. Marks, A.L. Boehman, D.A. Okrent, and A.P. Bentz, The Effects of Thermal Barrier Coatings on Diesel Engine Emissions, *J. Eng. Gas Turbines Power*, 1999, **121**(2), p 218-225
8. A.J. Modi, Experimental Study of Energy Balance in Thermal Barrier Coated Diesel Engine, *SAE International*, 2012, <https://doi.org/10.4271/2012-01-0389>
9. R. Kamo, N.S. Mavinahally, L. Kamo, W. Bryzik, and E.E. Schwartz, Injection Characteristics That Improve Performance of Ceramic Coated Diesel Engines, *SAE International*, 1999, <https://doi.org/10.4271/1999-01-0972>
10. T. Hejwowski and A. Weroński, The effect of Thermal Barrier Coatings on Diesel Engine Performance, *Vacuum*, 2002, **65**(3–4), p 427-432
11. S. Jaichandar and P. Tamilporai, Low Heat Rejection Engines—An Overview, *SAE International*, 2003, <https://doi.org/10.4271/2003-01-0405>
12. D. Zhu and R.A. Miller, Investigation of Thermal High Cycle and Low Cycle Fatigue Mechanisms of Thick Thermal Barrier Coatings, *Mater. Sci. Eng., A*, 1998, **245**(2), p 212-223
13. A. Kawaguchi, H. Iguma, H. Yamashita, N. Takada, N. Nishikawa, C. Yamashita, Y. Wakisaka, and K. Fukui, Thermo-Swing Wall Insulation Technology; A Novel Heat Loss Reduction Approach on Engine Combustion Chamber, *SAE International*, 2016, <https://doi.org/10.4271/2016-01-2333>
14. M. Andrie, S. Kokjohn, S. Paliwal, L.S. Kamo, A. Kamo, and D. Procknow, Low Heat Capacitance Thermal Barrier Coatings for Internal Combustion Engines, *SAE International*, 2019, <https://doi.org/10.4271/2019-01-0228>
15. S. Mahade, N. Curry, S. Björklund, N. Markocsan, P. Nylén, and R. Vaßen, Functional Performance of Gd₂Zr₂O₇/YSZ Multi-Layered Thermal Barrier Coatings Deposited by Suspension Plasma Spray, *Surf. Coat. Technol.*, 2017, **318**, p 208-216
16. M. Cuglietta, O. Arevalo-Quintero, and O. Kesler, Performance and Properties of Suspension Plasma Sprayed Metal-Supported Cu-Co-Ni-SDC SOFC Anodes in Methane, *Fuel Cells*, 2019, **19**(3), p 268-279
17. A. Ganvir, S. Joshi, N. Markocsan, and R. Vassen, Tailoring Columnar Microstructure of Axial Suspension Plasma Sprayed TBCs for Superior Thermal Shock Performance, *Mater. Des.*, 2018, **144**, p 192-208
18. A. Ganvir, R.F. Calinas, N. Markocsan, N. Curry, and S. Joshi, Experimental Visualization of Microstructure Evolution during Suspension Plasma Spraying of Thermal Barrier Coatings, *J. Eur. Ceram. Soc.*, 2019, **39**(2), p 470-481
19. K. Uchihara, M. Ishii, H. Nakajima, and Y. Wakisaka, A Study on Reducing Cooling Loss in a Partially Insulated Piston for Diesel Engine, *SAE International*, 2018, <https://doi.org/10.4271/2018-01-1276>
20. J.B. Heywood, *Internal Combustion Engine Fundamentals*, McGraw-Hill, New York, 1988
21. A. Ganvir, N. Curry, S. Björklund, N. Markocsan, and P. Nylén, Characterization of Microstructure and Thermal Properties of YSZ Coatings Obtained by Axial Suspension Plasma Spraying (ASPS), *J. Therm. Spray Technol.*, 2015, **24**(7), p 1195-1204
22. G. Moskal, L. Swadźba, M. Hetmańczyk, B. Witala, B. Mendala, J. Mendala, and P. Sosnowy, Characterization of Microstructure and Thermal Properties of Gd₂Zr₂O₇-Type Thermal Barrier Coating, *J. Eur. Ceram. Soc.*, 2012, **32**(9), p 2025-2034
23. N. Curry, K. VanEvery, T. Snyder, and N. Markocsan, Thermal Conductivity Analysis and Lifetime Testing of Suspension Plasma-Sprayed Thermal Barrier Coatings, *Coatings*, 2014, **4**(3), p 630-650
24. T.L. Bergman, D.P. DeWitt, F. Incropera, and A.S. Lavine, *Fundamentals of Heat and Mass Transfer*, Wiley, New York, 2011
25. J. Ekberg, A. Ganvir, U. Klement, S. Creci, and L. Nordstierna, The Influence of Heat Treatments on the Porosity of Suspension Plasma-Sprayed Yttria-Stabilized Zirconia Coatings, *J. Therm. Spray Technol.*, 2018, **27**(3), p 391-401

Publisher's Note Springer Nature remains neutral with regard to jurisdictional claims in published maps and institutional affiliations.